Cancer Immunology, Immunotherapy (2025) 74:151
https://doi.org/10.1007/s00262-025-04014-2

RESEARCH

Single-cell sequencing reveals tumor microenvironment features associated with the response to neoadjuvant immunochemotherapy in oral squamous cell carcinoma

Pu-Gen An[1,2,3] · Wen-Jie Wu[1,2,3] · Xiao Hu[1,2,3] · Zi-Qi Zhang[1,2,3] · Jie Zhang[1,2,3]

Received: 4 February 2025 / Accepted: 5 March 2025 / Published online: 19 March 2025

Abstract

Objectives In recent years, immune checkpoint inhibitors have shown promise as neoadjuvant therapies in the treatment of locally advanced oral squamous cell carcinoma (OSCC). However, the factors affecting the tumor response to immune checkpoint inhibitors (ICIs) remain unclear. This study aimed to analyze the impact of neoadjuvant chemoimmunotherapy (NACI) on the tumor microenvironment of OSCC via single-cell RNA sequencing, with the goal of optimizing treatment strategies.

Methods We analyzed biopsy, primary tumor, matched metastatic lymph node, and normal lymph node samples from four patients with OSCC receiving two cycles of tislelizumab (200 mg), albumin-bound paclitaxel (260 mg/m^2), and cisplatin (60–75 mg/m^2), with 3-week intervals between each cycle. This study explored the tumor microenvironment characteristics of tumors and metastatic lymph nodes in response to NACI.

Results We identified two major tumor cell subpopulations (C9 and C11), and patients with high expression of C11 subgroup-specific genes had a lower survival rate. FOXP3+ CD4 eTreg cells were found to potentially suppress the immune response. We found that NACI enhances antitumor immunity by promoting the proliferation of granzyme-expressing CD8+ T effector cells while simultaneously diminishing the effect of CD4+ T cells on Treg-mediated immune suppression. Furthermore, NACI was effective in suppressing inflammatory processes mediated by myeloid cells in tumors, contributing to its antitumor effects. The CCL19+ fibroblastic reticular cell (FRC) subgroup was significantly associated with the efficacy of NACI in patients with OSCC. We found that CCL19+ FRCs primarily exert their antitumor effects through interactions with CD8+ T lymphocytes via the –CXCL12−CXCR4 axis.

Conclusion We explored the immune landscape of primary OSCC tumors and metastatic lymph nodes in relation to clinical response to NACI. Our findings offer valuable insights into patient treatment responses and highlight potential new therapeutic targets for the future management of OSCC.

Keywords Oral squamous cell carcinoma · Neoadjuvant chemoimmunotherapy · Tumor microenvironment · CCL19+ fibroblastic reticular cell

Pu-Gen An and Wen-Jie Wu are co-first authors and contributed equally to this work.

✉ Jie Zhang
zhangjie123@bjmu.edu.cn

[1] Department of Oral and Maxillofacial Surgery, Peking University School and Hospital of Stomatology, No. 22 Zhongguancun South Avenue, Beijing 100081, People's Republic of China

[2] National Center of Stomatology and National Clinical Research Center for Oral Diseases, Beijing, People's Republic of China

[3] Central Laboratory, Peking University School and Hospital of Stomatology, Beijing, People's Republic of China

Abbreviations

CAF	Cancer-associated fibroblasts
CPS	Combined positive score
DC	Dendritic cell
DEG	Differentially expressed genes
ESCC	Esophageal squamous cell carcinoma
FRC	Fibroblastic reticular cells
GOBP	Gene Ontology biological process
ICIs	Immune checkpoint inhibitors
KEGG	Kyoto Encyclopedia of Genes and Genomes
LNM	Lymph node metastases
LNN	Normal lymph nodes
ORR	Objective response rate
OS	Overall survival

OSCC	Oral squamous cell carcinoma
MPR	Major pathological response
NACI	Neoadjuvant chemoimmunotherapy
pCR	Complete pathological response
PD-1	Programmed death-1
PD-L1	Programmed cell death ligand 1
PT	Primary tumor
scRNA-seq	Single-cell RNA sequencing
TCGA	The Cancer Genome Atlas
TPS	Tumor cell proportion score

Introduction

Head and neck squamous cell carcinoma (HNSCC) is the sixth most common cancer in the world. In 2022, 940,000 new cases and 450,000 deaths were reported. The incidence of HNSCC continues to rise, and it is estimated to increase by 30% by 2030, which translates to 1.08 million new cases each year [1]. HNSCC, especially oral squamous cell carcinoma (OSCC), has a poor prognosis. According to research statistics, the 5-year overall survival rate for patients increased from 55% from 1992–1996 to 66% from 2002 to 2006 [2]. For locally advanced resectable OSCC, surgical resection followed by adjuvant radiotherapy or postoperative concurrent chemoradiotherapy is the standard treatment regimen. However, the 5-year overall survival rate for these patients remains at 40–50% [3, 4]. Although combined induction therapy including cisplatin, docetaxel, and 5-fluorouracil (TPF) has been extensively studied, a phase III clinical trial revealed that definitive radiotherapy or preoperative induction chemotherapy did not significantly improve survival in patients with locally advanced HNSCC. Furthermore, phase III trials of induction chemotherapy with docetaxel, cisplatin, and fluorouracil did not yield positive results in patients with locally advanced resectable OSCC. Therefore, this standard treatment has failed to provide substantial survival benefits for HNSCC patients [5–7], so there is an urgent clinical need to explore new and effective treatment methods to improve patient survival.

In recent years, immune checkpoint inhibitors (ICIs), which include programmed cell death protein 1 (PD-1) and its ligand programmed cell death ligand 1 (PD-L1), have become promising new adjunctive treatment strategies for solid tumors such as breast cancer, lung cancer, and esophageal squamous cell carcinoma (ESCC) [8–11]. Moreover, for recurrent or metastatic HNSCC, PD-1 inhibitors have been approved by the Food and Drug Administration (FDA) as first-line treatments. In the KEYNOTE-048 trial, the objective response rate (ORR) for the pembrolizumab monotherapy group was 17%, whereas the ORR for the pembrolizumab combined with chemotherapy group was 36% [12]. For primary locally advanced HNSCC, several clinical trials have shown that administering neoadjuvant anti-PD-1 monoclonal antibodies in combination with chemotherapy before surgery can significantly improve the pathological response rate, prolong progression-free survival, and maintain an acceptable safety profile and feasibility [13, 14]. However, despite the encouraging clinical outcomes observed with neoadjuvant anti-PD-1 monoclonal antibodies combined with chemotherapy, the major pathological response (MPR) rate ranges from 60 to 70%, and the complete pathological response (pCR) rate is between 30 and 50% [15–18]. Many patients develop resistance and are unable to benefit from ICI treatment. Therefore, an in-depth investigation of the mechanisms underlying the neoadjuvant chemoimmunotherapy (NACI) response in HNSCC and the identification of biomarkers that reflect the complex interactions between tumors and the immune system will be key to personalizing effective patient stratification and improving the pCR rate.

Single-cell RNA sequencing (scRNA-seq) is a cutting-edge technology used to study the tumor microenvironment and is capable of revealing tumor heterogeneity, immune invasion, and epithelial−mesenchymal transition at the single-cell level. In this study, we employed single-cell sequencing to analyze primary locally advanced OSCC, matched lymph node metastases (LNM) and normal lymph nodes (LNN), to reveal alterations in the tumor microenvironment characteristics of HNSCC following neoadjuvant chemotherapy. This research will establish a basis for identifying potential therapeutic targets for OSCC and may have significant implications for addressing immune resistance in OSCC patients.

Methods

Patients

We obtained biopsy (before NACI), primary tumor (after NACI), and matched LNM and LNN samples from four patients who received two cycles of NACI, consisting of tislelizumab, albumin-bound paclitaxel and cisplatin, every 3 weeks. After NACI, patients underwent surgery and adjuvant radiotherapy or concurrent chemoradiotherapy. The basic information of these four patients is provided in Supplementary Table 1 (Table S1). Notably, the metastatic lymph nodes of patient P1 did not pass quality control.

Tissue dissociation and single-cell suspension preparation

The collected samples were transferred to Petri dishes prefilled with 1 × PBS (without RNase or Ca^{2+}/Mg^{2+} ions), which were kept on wet ice. The tissue was washed with 1 × PBS to remove blood, oils, and other surface

contaminants. Each tissue was subsequently cut into small pieces of approximately 0.5 mm^2. Next, the cut tissue was washed again with 1 × PBS, and the cleaned tissue fragments were added to a dissociation solution containing 0.35% collagenase IV, 2 mg/ml papain, and 120 Units/ml DNase I. The mixture was placed in a 37 °C water bath shaker at 100 rpm for 20 min. Next, 1 × PBS containing 10% fetal bovine serum (FBS) was added to terminate the digestion, and the solution was gently pipetted up and down 5–10 times to avoid excessive shear stress, leading to cell death. The resulting cell suspension was filtered through a 70–30 μm cell strainer. The suspension was then centrifuged at 300 × g for 5 min at 4 °C, and the cell pellet was collected and resuspended in 100 μl of 1 × PBS (0.04% BSA).

To remove red blood cells, 1 ml of 1 × red blood cell lysis buffer (MACS 130–094–183, 10 ×) was added, and the mixture was incubated at room temperature or on wet ice for 2–10 min. After lysis, the mixture was centrifuged at 300 × g for 5 min at 4 °C, and the cell pellet was collected. Next, 100 μl of a dead cell removal reagent [Dead Cell Removal MicroBeads (MACS 130–090–101)] was added and mixed thoroughly. The mixture was incubated at room temperature for 15 min, after which binding buffer was added, and the suspension was passed through MS Columns (130–042–201) to remove the reagent and dead cells. The cells were then collected by centrifugation at 300 × g for 5 min at 4 °C, and the cell pellet was resuspended in 1 × PBS (0.04% BSA). This centrifugation step was repeated twice.

After the completion of tissue dissociation, red blood cell lysis, and dead cell removal, the candidate cells were resuspended in 100 μl of 1 × PBS (0.04% BSA) to create a cell suspension. Cell viability was assessed via the trypan blue exclusion method, with a requirement for viability > 85%. The cell count was determined using a hemocytometer or an automated cell counter (Countess II Automated Cell Counter), with a target cell concentration of 700–1200 cells/μl.

Chromium 10 × genomic library construction and sequencing

According to the instructions of the 10 × Genomics Chromium Single-Cell 3' Kit (V3), the single-cell suspension was loaded onto a 10 × Chromium chip, with an expected capture of 8000 single cells. cDNA amplification and library construction were performed following the standard protocol. The library was sequenced by LC-Bio Technology Co., Ltd. (Hangzhou, China) using an Illumina NovaSeq 6000 sequencing system (paired-end sequencing, 150 bp), with a sequencing depth of at least 20,000 reads per cell.

Bioinformatics analysis

The vast majority of bioinformatics data analyses were conducted using the R software (version 4.3.3). The results from the Illumina sequencing platform were converted to FASTQ format via bcl2fastq software (version 2.20). The scRNA-seq data were aligned to the reference genome via CellRanger software (version 8.0.1); this software was also used to identify and quantify the cells and individual 3' end transcripts in the sequenced samples (https://support.10xgenomics.com/single-cell-gene-expression/software/pipelines/latest/what-is-cell-ranger, version 7.0.0). The output data from CellRanger were imported into Seurat (version 5.1.0) for filtering low-quality cells, dimensionality reduction, and clustering of the scRNA-seq data. The filtering criteria for low-quality cells were as follows: the number of genes expressed per cell was greater than 500, and the proportion of mitochondrial genes expressed in the cells was less than 25%. The cells were then projected into 2D space via UMAP. This process included the following steps:

1. The "NormalizeData" function in Seurat with the LogNormalize method was used to calculate gene expression values.
2. Principal component analysis (PCA) was performed using the normalized expression values, with the first 20 principal components (PCs) utilized for clustering analysis via FindClusters.
3. The marker genes for each cluster were identified via FindAllMarker analysis, and the filtering criteria for the marker gene set were as follows: expression in more than 10% of the cells within each cluster, a P value ≤ 0.01, and a gene expression fold change (logFC) ≥ 0.26.

The quality control for scRNA-seq is as follows: cells were filtered based on nFeature_RNA and nCount_RNA using 3 median absolute deviations (MADs). Cells were retained if they exhibited percent.mt < 10 and percent.hb < 5. Doublets were removed utilizing scDblFinder v1.16.0. Integrative analysis was performed by Harmony within Seurat, with 30 principal components (PCs) set as the default. The FindAllMarker function was applied with the parameters min.pct = 0.25 and logfc.threshold = 0.25.

Additionally, differentially expressed genes (DEGs) obtained from the FindAllMarkers analysis comparing each cluster to the other clusters were subjected to Gene Ontology (GO) and Kyoto Encyclopedia of Genes and Genomes (KEGG) enrichment analysis via hypergeometric testing. We utilized clusterProfiler (version 4.10.1) for KEGG and GOBP pathway analysis. And the cell interaction analysis was performed using CellChat (version 2.1.2). Preliminary cell type annotation was performed

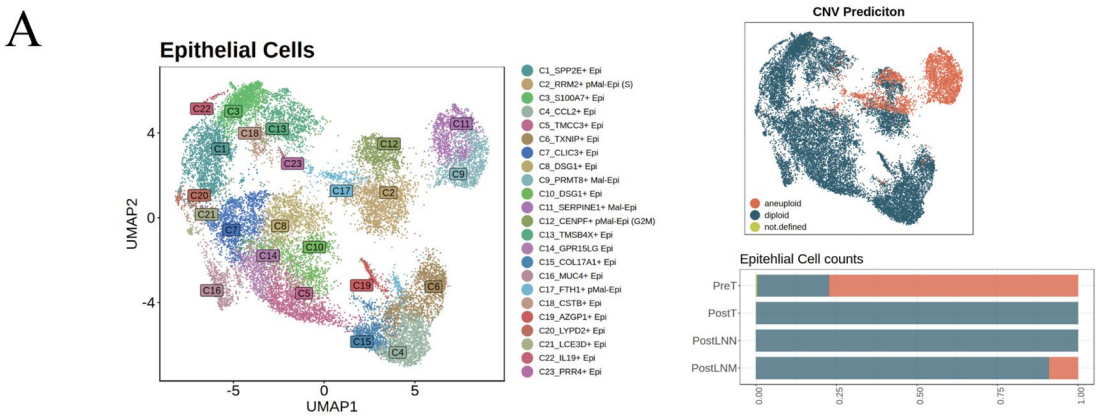
A
Epithelial Cells
UMAP1
UMAP2
C1_SPP2E+ Epi
C2_RRM2+ pMal-Epi (S)
C3_S100A7+ Epi
C4_CCL2+ Epi
C5_TMCC3+ Epi
C6_TXNIP+ Epi
C7_CLIC3+ Epi
C8_DSG1+ Epi
C9_PRMT8+ Mal-Epi
C10_DSG1+ Epi
C11_SERPINE1+ Mal-Epi
C12_CENPF+ pMal-Epi (G2M)
C13_TMSB4X+ Epi
C14_GPR15LG Epi
C15_COL17A1+ Epi
C16_MUC4+ Epi
C17_FTH1+ pMal-Epi
C18_CSTB+ Epi
C19_AZGP1+ Epi
C20_LYPD2+ Epi
C21_LCE3D+ Epi
C22_IL19+ Epi
C23_PRR4+ Epi
CNV Prediciton
aneuploid
diploid
not.defined
Epitehlial Cell counts
PreT
PostT
PostLNN
PostLNM

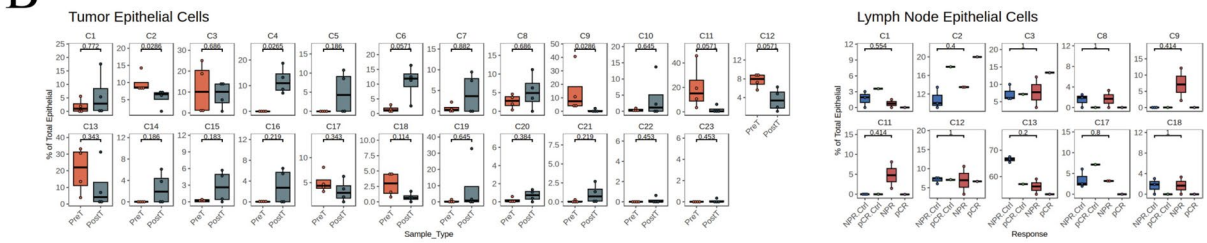
B
Tumor Epithelial Cells
% of Total Epithelial
Sample_Type
Lymph Node Epithelial Cells
Response

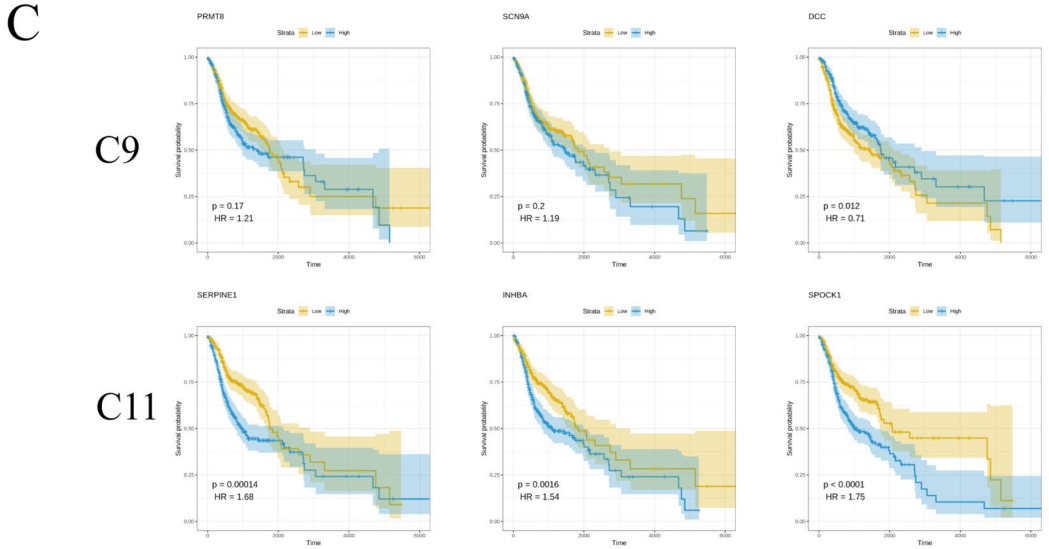
C
C9
C11
PRMT8
SCN9A
DCC
SERPINE1
INHBA
SPOCK1
p = 0.17
HR = 1.21
p = 0.2
HR = 1.19
p = 0.012
HR = 0.71
p = 0.00014
HR = 1.68
p = 0.0016
HR = 1.54
p < 0.0001
HR = 1.75

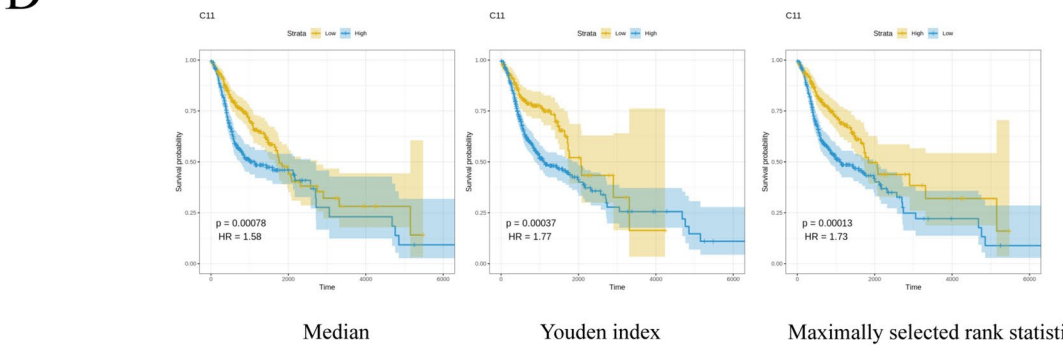
D
C11
p = 0.00078
HR = 1.58
p = 0.00037
HR = 1.77
p = 0.00013
HR = 1.73
Median
Youden index
Maximally selected rank statistics

◂**Fig. 1** **A** UMAP plot of epithelial cells used to visualize the single-cell landscape on the basis of marker genes. **B** Proportion of 23 epithelial cell clusters in primary tumors, normal lymph nodes (LNNs), and metastatic lymph nodes (LNMs) after neoadjuvant chemoimmunotherapy (NACI). **C** Survival curves of patients in the TCGA-HNSC cohort grouped according to the expression levels of C9 and C11 marker genes. **D** The top 50 DEGs with high expression in the C11 cell cluster were used to construct a composite scoring system. Survival curves of patients in the TCGA-HNSCC cohort grouped according to the median expression levels of genes in this scoring system; Youden's index and the maximum selection rank statistic are provided

using SingleR (version 2.4.1) and celldex (version 1.12.0.) HumanPrimaryCellAtlasData and BlueprintEncodeData in the celldex package were used as references. All the final cell type annotation in the manuscripts were then curated manually, based on our prior knowledge and published literatures.

Survival analysis

Bulk RNA-seq data of The Cancer Genome Atlas (TCGA)-HNSC was retrieved using TCGAbiolinks (version 2.32.0) from the TCGA database (https://portal.gdc.cancer.gov/). Downstream analysis was performed on the group 'Primary Tumor' and 518 samples were analyzed. Top 50 DEGs from C9 and C11 were calculated for GSVA enrichment score for each sample using GSVA v1.52.3. To assess the relationship between the target gene sets and patient prognosis, the single-sample gene set enrichment analysis method was employed to calculate scores for each gene set within the samples. The samples were subsequently assigned to high expression or low-expression groups, and the median enrichment score was used as the cutoff point. The Kaplan−Meier curves were generated using R packages survival and survminer for the visualization of differences in overall survival rates between the high expression and low-expression groups for each gene set.

Results

Cluster analysis of epithelial cells

After quality control, we obtained a total of 20,624 epithelial cells. To visualize the single-cell landscape from the sequencing data, we employed unsupervised clustering analysis to classify the epithelial cells into 23 distinct cell types (Fig. 1A). Among the epithelial cells, tumor cells exhibiting aneuploidy were detected, primarily in the pretreatment primary lesions and in the posttreatment lymph node metastasis (PostLNM) samples; no aneuploid tumor cells were identified in the posttreatment tumor (PostT) samples and posttreatment normal lymph node (PostLNN) samples (Fig. 1A).

The epithelial cells were classified into 23 clusters, of which 2 were designated tumor cells (Mal, malignant; with aneuploid cell proportions of 98.71% in cluster C9 and 98.37% in cluster C11). Three clusters were defined as partially malignant cells (pMal, partially malignant; with aneuploid cell proportions of 27.26% in cluster C2, 34.36% in cluster C12, and 47.16% in cluster C17). Additionally, 11 clusters contained a small number of tumor cells (mMal, minimally malignant; four clusters (C6, C8, C13, C15) had aneuploid cell proportions between 1 and 10%, and seven clusters (C1, C3, C7, C16, C18, C20, C21) had proportions of less than 1%. Next, we focused on tumor cells and partially malignant cells (Fig. S1A).

In the biopsy samples, clusters C9 and C11 represented the primary tumor cells. Following neoadjuvant therapy, these two populations of malignant tumor cells in the primary tumor samples nearly completely disappeared. However, these cell populations were significantly more abundant in LNMs than in matched LNN in patients with a non-major pathological response (NPR), whereas in patients with a complete pathological response (pCR), these cell populations were completely absent. Clusters C2, C12, and C17 exhibited significantly decreased enrichment following neoadjuvant therapy (Figs. 1B, S1A).

The top 20 highly expressed genes in C9 and C11 (Fig. S1B) were used to group patients for survival analysis. Survival curve analysis of the TCGA-HNSCC cohort revealed that high expression of genes (*SERPINE1*, *INHBA*, *SOPCK1*) in cluster C11 was associated with a shorter survival time, suggesting that this type of cell may be closely related to survival outcomes. In contrast, the characteristic genes (*PRMT8*, *SCN9A*, *DCC*) that are highly expressed in the C9 cell cluster do not exhibit a significant correlation with patient survival outcomes (Fig. 1C). Additionally, we constructed a comprehensive scoring model using the top 50 DEGs for C11. In the TCGA-HNSCC general transcriptome, patients with high score of these cell-enriched gene presented significantly shorter survival times (Fig. 1D). The top 20 highly expressed genes in clusters C2, C12, and C17 are presented in Fig. S1C. Clusters C2 and C12 represent proliferative cells that highly express cell cycle genes, indicating that these tumor cells may be sensitive to cell cycle inhibitors (Fig. S1D). Cluster C17 lacks specific gene markers while exhibiting high expression of various markers characteristic of both tumor and normal cells.

To further explore the functional roles of the two primary malignant cell clusters, we conducted an enrichment analysis of cellular signaling pathways on the basis of Gene Ontology biological process (GOBP) and KEGG pathways (Fig. S2). The results revealed that C9 was associated primarily with "nonmotile cilium assembly", "negative regulation of cell projection organization", and "embryonic organ

morphogenesis". C11 was linked to pathways such as the "PI3K-Akt signaling pathway", "ECM-receptor interaction", "protein digestion and absorption", "proteoglycans in cancer", and "human papillomavirus infection", as well as processes such as "extracellular matrix organization", "endocytosis", "regulation of cell migration", and "cell adhesion". Given that C11 primarily expresses genes related to the PI3K signaling pathway, it is likely that PI3K inhibitors may be particularly effective against this malignant cell population.

Characteristics of T lymphocyte remodeling induced by NACI

T cells were divided into 24 cell populations on the basis of the expression of typical marker genes for T lymphocytes. Among them, the number of T lymphocytes in the lymph nodes was significantly greater than that in the primary tumor. CD8+ T lymphocytes play a central role in immunotherapy. Five clusters of CD8+ T lymphocytes were identified: C1 and C18 effector T cells, C11 exhausted T cells, C13 memory T cells, and C17 naïve T cells (Fig. 2A). The CD8 Teff (C1 and C18) clusters highly expressed granzymes (*GZMK* and *GZMA*) and *KLRG1*, which are CD8 cytotoxic gene markers, suggesting their effector function (Fig. 2B). CD8 Tex (C11) cells highly expressed granzymes (*GZMB*, *GZMA, GZMH*), *IFNG*, coinhibitory receptors (*PDCD1*, *LAG3*, *TIGIT*, *HAVCR2*) and exhaustion markers (*TOX*, *ENTPD1*), which are CD8 exhaustion, cytotoxic, and effector gene markers (Fig. 2A). The C13 and C17 subsets primarily expressed *IL7R*, *S1PR1*, *TCF7*, *LEF1*, and *SELL* markers, which are naïve and memory cell gene markers (Fig. 2A).

After neoadjuvant therapy, the population of CD8+ T lymphocytes significantly increased in the primary tumor. Among them, the proportions of cells in C1 and C18 clusters, which represent CD8 effector T cells, markedly increased. Notably, in LNMs from the pCR group, there was also an increase, whereas in LNMs of the NPR-pCR group, these two effector CD8+ T-cell subsets did not significantly increase. The proportion of C13 cells was higher in the primary tumor after neoadjuvant therapy, and its proportion in LNMs of the pCR group was greater than that in the matched LNNs No significant differences were observed in the C11 and C17 subsets after neoadjuvant therapy. The distribution of these CD8+ T-cell subsets and their associations with MPR/pCR suggest that the cytotoxicity and proliferation of CD8+ T cells play important roles in the response to NACI in HNSCC.

We identified a total of 14 subsets of CD4+ T cells. In the primary tumor, the C5 FOXP3+ effector Treg (eTreg) cluster significantly decreased after neoadjuvant therapy, and a similar reduction was observed in the LNMs of the pCR group. However, there was an increasing trend in the LNMs of the NPR group following neoadjuvant therapy. This observation aligns with findings from studies on lung cancer [19] and colorectal cancer [20]. These findings indicate that anti-PD-1 monoclonal antibodies can reduce the effect of Tregs in responsive tumors. This cell subset expresses high levels of various immunosuppressive receptors, such as *CTLA4*, *TIGIT*, and *TNFRSF18*, which can inhibit antitumor immunity. In summary, these results suggest that successful ICI therapy suppresses the immunosuppressive effects mediated by CD4+ T cells by decreasing the proportion of Tregs.

NACI alters the characteristics of B lymphocytes

B cells were categorized into 14 clusters on the basis of the characteristic marker genes of B lymphocytes. CD20+ B cells constitute a heterogeneous subset consisting of naïve B (Bn), memory B (Bm), and germinal center (Bgc) subsets with different transcriptional profiles (Fig. 3A). Following neoadjuvant therapy, there was an increase in the proportion of Bgc cells and plasma cells, with C7 memory B cells also increasing. After neoadjuvant therapy, the C9-MKI67+ DZ Bgc cell subset increased in the primary tumor, and the proportion in the pCR-group LNM samples was greater than that in the matched LNN samples, whereas no significant differences were observed in the NPR group. Additionally, the proportion of C7-COL4A3+ Bm cells was increased after neoadjuvant therapy (Fig. 3B). To further explore the interactions between B cells and CD8+ T cells, we utilized the CellChat analysis to reveale a close relationship between C9 and CD8+ T effector cells that exert antitumor effects, suggesting that this group of cells may promote antitumor activity by interacting with CD8+ T cells following neoadjuvant therapy. GOBP functional analysis of C7 cells revealed an association with the activation and differentiation of CD4 helper T cells (Fig. 3C). These findings suggest that immunotherapy may facilitate the recovery of the memory function of B cells while promoting the activation and differentiation of CD4 helper T lymphocytes.

NACI decreased the proinflammatory program in myeloid cells

Using characteristic cell marker genes, we categorized myeloid cells into 20 cell clusters. As illustrated, the neutrophil population was primarily concentrated in the primary tumor (Fig. 4A). Following neoadjuvant therapy, there was a significant increase in the number of dendritic cells (DCs) and a notable decrease in the neutrophil count. The DCs were divided into four subsets, with each subset showing an increase in the primary tumor, although these changes did not reach statistical significance. Similarly, no significant differences were observed in LNMs compared

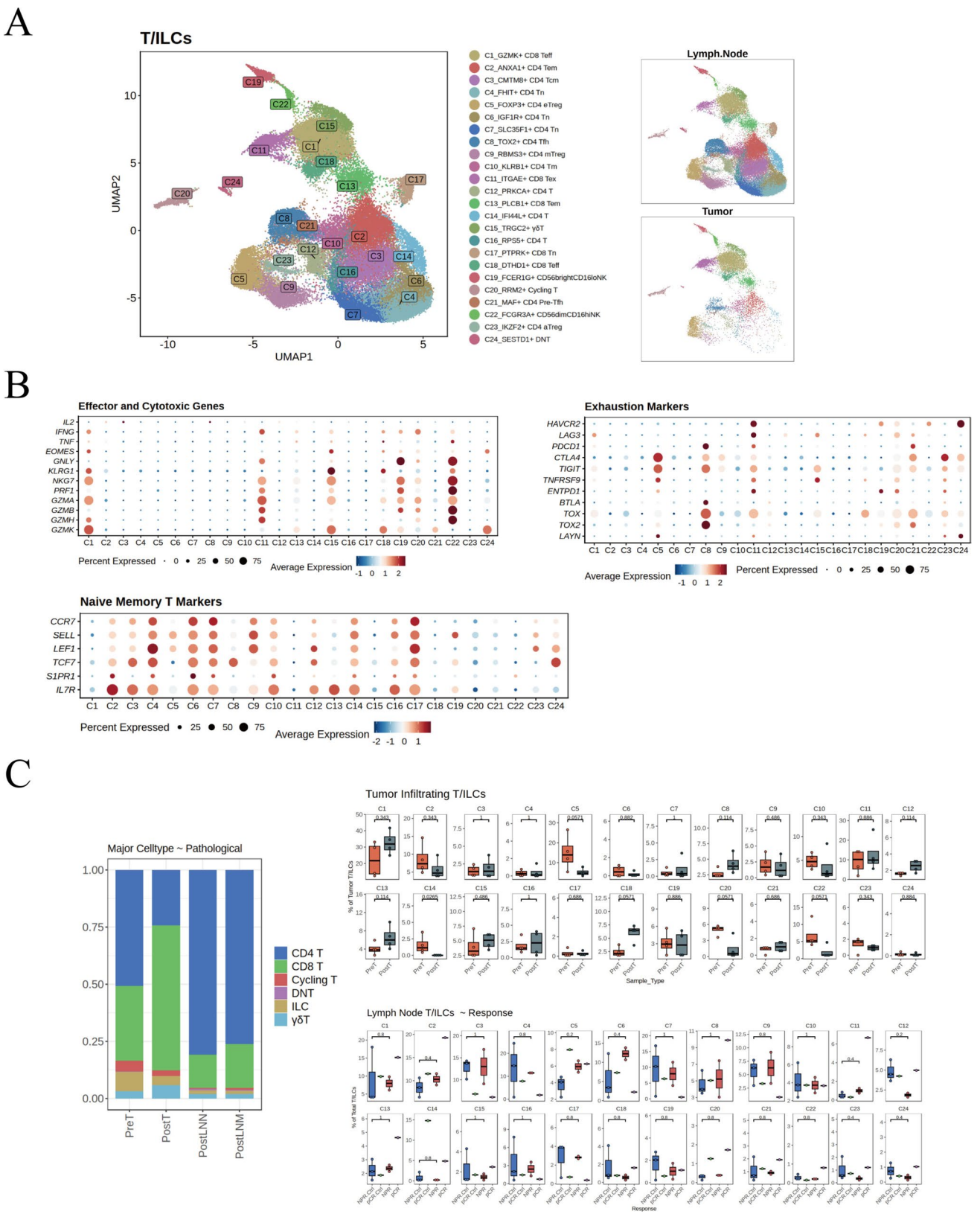

Fig. 2 **A** UMAP plot of T cells showing the single-cell landscape on the basis of marker genes. **B** Expression levels of marker genes for the 24 T-cell clusters. **C** Proportions of 24 T lymphocyte cell clusters in the primary tumors, LNNs, and LNMs after NACI

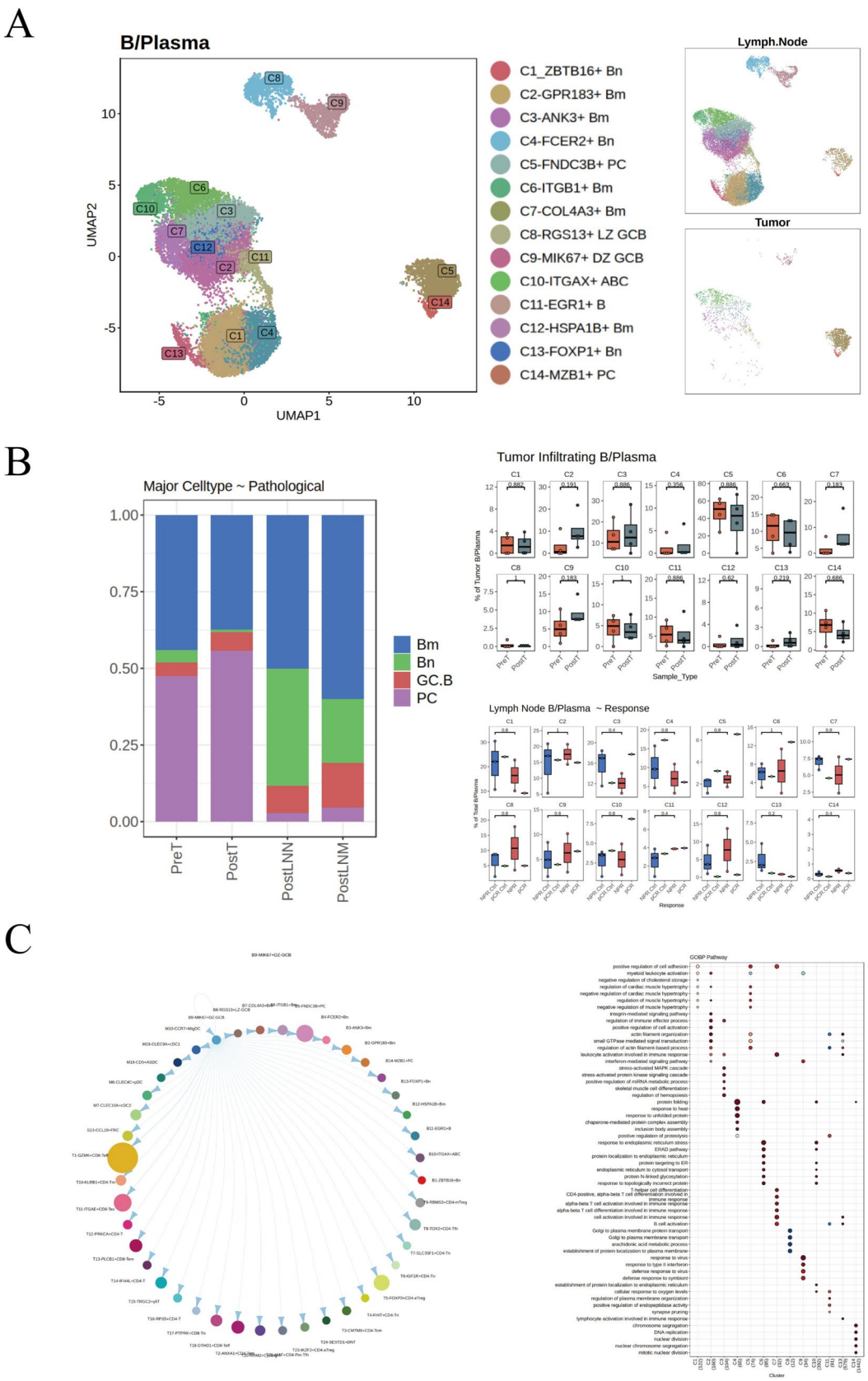
A
B/Plasma
C1_ZBTB16+ Bn
C2-GPR183+ Bm
C3-ANK3+ Bm
C4-FCER2+ Bn
C5-FNDC3B+ PC
C6-ITGB1+ Bm
C7-COL4A3+ Bm
C8-RGS13+ LZ GCB
C9-MIK67+ DZ GCB
C10-ITGAX+ ABC
C11-EGR1+ B
C12-HSPA1B+ Bm
C13-FOXP1+ Bn
C14-MZB1+ PC
Lymph.Node
Tumor
UMAP1
UMAP2
B
Major Celltype ~ Pathological
Bm
Bn
GC.B
PC
PreT
PostT
PostLN
PostLNM
Tumor Infiltrating B/Plasma
% of Tumor B/Plasma
Sample_Type
Lymph Node B/Plasma ~ Response
% of Total B/Plasma
Response
C
GOBP Pathway
Cluster

◂**Fig. 3** **A** UMAP plot of B cells showing the single-cell landscape on the basis of marker genes. **B** Proportion of 14 B lymphocyte cell clusters in primary tumors, LNNs, and LNMs after NACI. **C** Communication between C9-MIK67+ DZ Bgc cells and other cell subpopulations. Pathway enrichment analysis of B lymphocyte subpopulations via GOBP

with LNNs (Fig. 4B). In primary tumors, the proportions of C4-CXCR4-neutrophils, C16-PROK2-neutrophils, and C11-CCL3L3-neutrophils were significantly reduced (Fig. 4B). Among these, C4 exhibited high expression of the neutrophil chemokines *CXCR4*, *CCL3L3*, and *CCL4L2* (Fig S4A). To further explore the functions of these three clusters of neutrophils, we conducted GO and KEGG enrichment analyses of cellular signaling pathways. The results indicated that C4-CXCR4-neutrophils were primarily associated with "oxidative phosphorylation", "chemical carcinogenesis—reactive oxygen species", "proton transmembrane transport", and "response to oxidative stress". C16-PROK2-neutrophils were found to be linked to pathways such as "leukocyte cell–cell adhesion", "cellular response to biotic stimulus", "NF-kappa B signaling pathway", "IL-17 signaling pathway" and "TNF signaling pathway".

Inflammation is associated with the development of cancer and its response to treatment [21]. In this study, the proportions of three neutrophil subsets with proinflammatory functions were significantly reduced following neoadjuvant therapy. This reduction may contribute to the ability of NACI to modulate inflammatory processes within the tumor, thereby exerting antitumor effects.

CCL19+ fibroblastic reticular cells (FRCs) communicate with T cells through the CXCL12–CXCR4 axis to exert antitumor effects

On the basis of the characteristic marker genes of stromal cells, the stroma was divided into 23 cell clusters. Following neoadjuvant therapy, the endothelial cell population significantly increased. A total of five subsets of endothelial cells were identified (Fig. 5A). C2 is an endothelial cell subset that expresses the *ACKR1* gene at a high level, which significantly increases after neoadjuvant therapy. Similarly, compared with LNNs, LNMs from patients with a pCR also exhibited a significant increase in the proportion of C2 cells (Fig. 5B). This subset of cells expresses high levels of genes such as *ACKR1*, *CCL14*, and *SELP*, and its primary function is to regulate the migration of leukocytes across the vascular wall (Fig. S5A, B). C16 consists of endothelial cells that express the *SEMA3G* gene, as well as other genes, such as *NEBL* and *PLLP*, at a high level. Its functions are associated mainly with epithelial cell migration, angiogenesis, and endothelial cell differentiation (Fig. S5A, B). After neoadjuvant therapy, this proportion of this subset of cells significantly increased; however, no notable differences were observed when LNMs were compared with LNN (Fig. 5B).

A total of 11 clusters of fibroblasts were identified. Fibroblasts exhibit significant heterogeneity. In primary tumors, after neoadjuvant therapy, the proportions of clusters C7, C8, C11, and C15 significantly increased. However, compared with LNNs, LNMs tended to have decreased proportions of clusters C7 and C8, with no difference observed for C11. For cluster C15, there was no significant trend in LNMs from the NPR group, whereas the proportions of these cells were significantly decrease in LNMs from the pCR group (Fig. 5B). Subclusters C3 and C4 were enriched in primary tumors after neoadjuvant therapy and were also present in greater numbers in LNMs than in LNNs. Conversely, the proportions of clusters C1, C10, and C20 were significantly decreased in primary tumors after neoadjuvant therapy; however, they exhibited an increasing trend in LNMs compared with LNNs (Fig. 5B). It has been reported that the C1 and C20 cell subsets, along with MMP+ fibroblasts, promote the formation of an immunosuppressive tumor microenvironment through their interactions with regulatory T cells [22]. There was no significant difference in the proportion of the C18 cell subset before and after neoadjuvant therapy. The functional pathways enriched in the aforementioned cell subsets are shown in Fig. S5B.

C13 represents a subset of fibroblastic reticular cells that express high levels of CCL19. Following neoadjuvant therapy in primary tumors, the abundance of these cells significantly increased. In contrast, C13 cells were found to be present in lower proportions in LNMs than in LNNs in the NPR group, while there was notable upregulation in LNMs in the pCR group. CellChat analysis revealed that after neoadjuvant therapy, C13-CCL19+ FRCs exhibited more interactions with memory CD4+ T cells and naïve CD4+ T lymphocytes mediated by the CCL19-CCR7 axis (Figs. 5C, S6A). Furthermore, C13-CCL19+ FRCs interacted with other cells via the CXCL12–CXCR4 axis; specifically, these FRCs interacted with nearly all CD4+ T and CD8+ T lymphocytes, as well as almost all B cells, with a particularly significant enrichment in interactions with CD8+ T cells (Figs. 5C, S6B). These findings suggest that NACI may promote the proliferation of CCL19+ FRCs, which, in turn, may facilitate the recruitment of T lymphocytes through the CXCL12–CXCR4 axis, thereby exerting an antitumor effect.

In summary, these results highlight the important role of stromal cells in lymphocyte chemotaxis and the resolution of protumor inflammation during ICI-mediated immune remodeling.

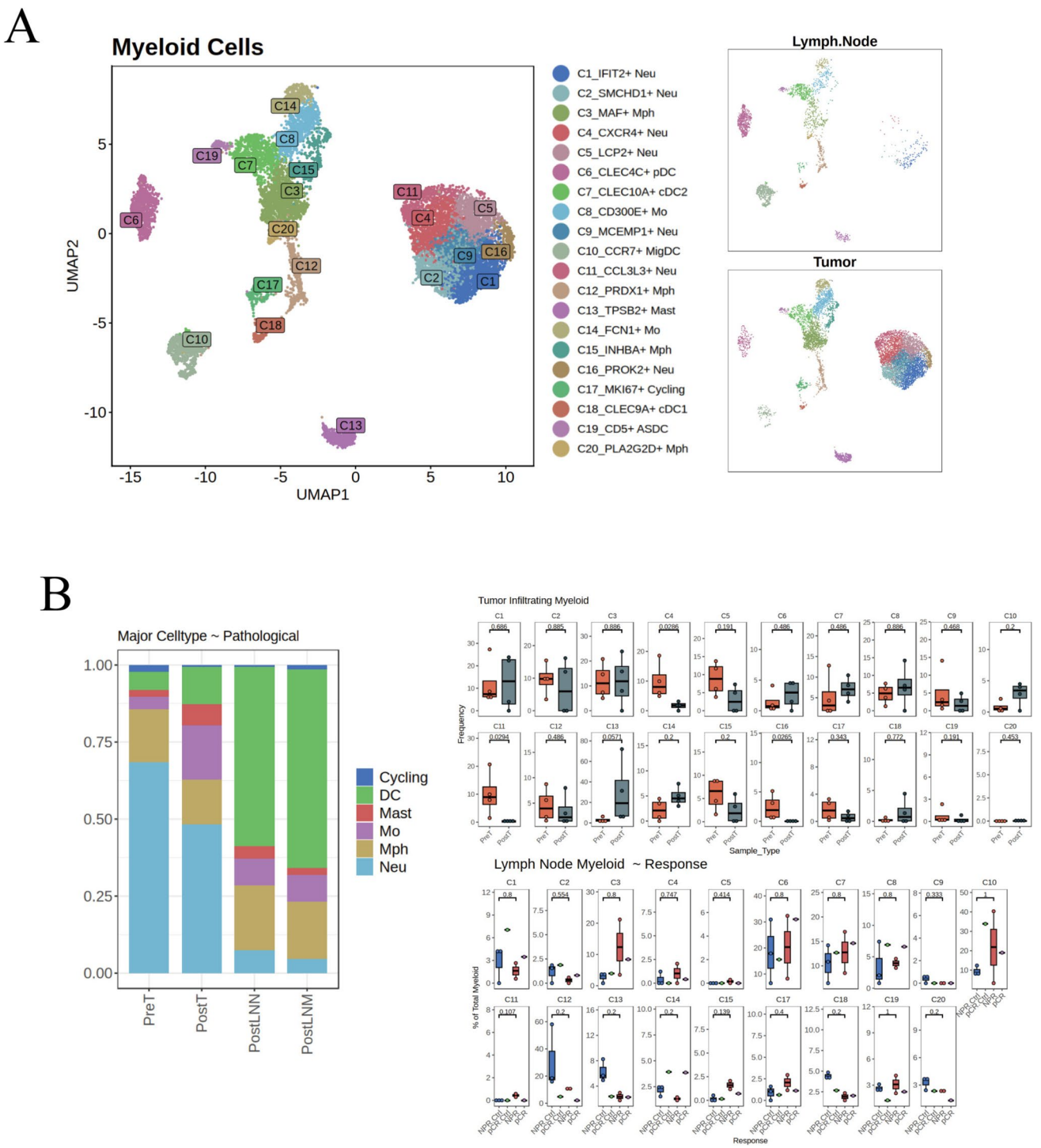

Fig. 4 **A** UMAP plot of myeloid cells showing the single-cell landscape on the basis of marker genes. **B** Proportions of 20 myeloid cell clusters in primary tumors, LNNs, and LNMs after NACI

Discussion

In recent years, NACI has emerged as a promising therapeutic approach for HNSCC patients. Although NACI has shown encouraging therapeutic effects in clinical settings [15, 16], its mechanism of action and the reasons for immune resistance in patients remain unclear. To reveal the mechanisms underlying sensitivity and resistance to NACI in HNSCC patients, we employed scRNA-seq to uncover

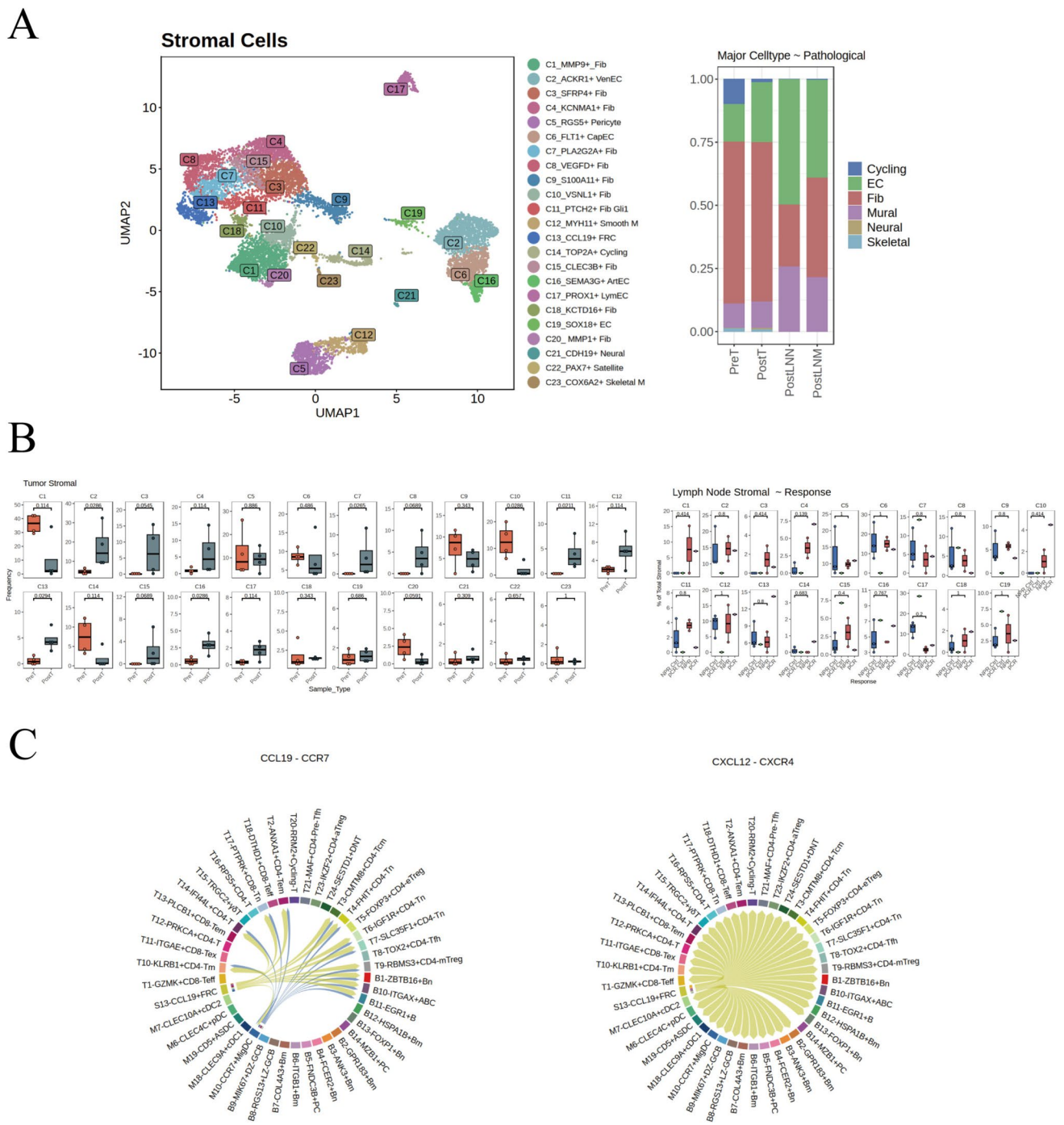

Fig. 5 **A** UMAP plot for stromal cells showing the single-cell landscape on the basis of marker genes. **B** Proportions of 23 stromal cell clusters in primary tumors, LNNs, and LNMs after NACI. **C** Intercellular communication between C13-CCL19+ FRCs and T-cell clusters, B-cell clusters, and myeloid cell clusters on the basis of the CCL19-CCR7 axis and the CXCL12–CXCR4 axis

the dynamic changes in the tumor microenvironment and its correlation with pathological responses to NACI.

First, we observed that after NACI treatment, the C11 subpopulation in the primary tumors of patients who achieved a pCR nearly completely disappeared. In contrast, C11 remained abundant in the LNMs of patients in the NPR group. Furthermore, the high expression of genes associated with this malignant cell population was closely correlated with survival, indicating that the poor pathological response of metastatic lymph nodes related to C11 is associated with an unfavorable patient prognosis. NACI significantly increased the infiltration of CD8+ effector T

cells while reducing the number of FOXP3+ eTregs. The infiltration of CD8+ T cells is one of the key factors for the success of immune checkpoint therapy [23, 24], while the high tolerance induced by CD4+ Tregs is a major factor contributing to tumor immune evasion [25]. In LNMs from patients in the NPR group, the number of FOXP3+ eTregs increased, indicating that immunosuppression developed in these lymph nodes. Additionally, in our study, primary tumors from patients with a pathological response of MPR exhibited lower proportions of neutrophils associated with proinflammatory pathways and higher proportions of DC cells. Tumor-associated neutrophils can differentiate into a cytotoxic antitumor N1 state and an immunosuppressive protumor N2 state. Although specific data regarding their roles in HNSCC remain relatively scarce, published studies have indicated that higher tumor T stage is associated with increased neutrophil infiltration [26].

Cancer-associated fibroblasts (CAFs) are the most abundant nonimmune cell type in the tumor microenvironment and have been shown to support tumor cell proliferation, invasion, and metastasis, thereby promoting tumor development [27, 28]. Consistent with these findings, our study revealed that the number of C1, C10, and C20 populations, defined as CAFs, significantly decreased after NACI. However, we also observed an increase in certain fibroblast subpopulations (C7, C8, C11, and C15) following treatment. Accumulating evidence suggests that fibroblasts may acquire antitumor properties during the early stages of tumor development [29–31]. The transition from the natural protective role of human cells of connective origin in response to the needs of tissue repair and regeneration to changes in tumor stromal fibroblasts may involve important initial antitumor properties. Ultimately, this balance is disrupted, leading to the occurrence and progression of tumors [32]. Exploring targeted therapies that can selectively modulate CAF activity or enhance the antitumor functions of specific fibroblast populations could pave the way for innovative treatment approaches.

Interestingly, we identified a population of FRCs that express high levels of CCL19 within primary tumors, and the proportions of these cells significantly increased following NACI. In contrast, the proportions of these cells were reduced in LNMs from patients in the NPR group, indicating its potential antitumor role. Studies have shown that FRCs in lung cancer can promote protective antitumor immune responses [33]. In tumor-draining lymph nodes, CCL19+ FRCs facilitate the activation and expansion of antitumor CD8+ T cells and guide these T cells to migrate to the tumor parenchymal area. Additionally, they can recruit activated tumor-specific stem cell-like T cells to migrate to tertiary lymphoid structures. The initiation of tumor antigen-specific T-cell responses is key to the successful control of immunogenic tumors [34, 35]. In this study, the proportions of CCL19+ FRCs were found to be low in LNMs in the NPR group, suggesting that the role of this cell population in the interplay between tumor-draining lymph nodes and the tumor may be key to investigating NACI resistance.

The limitations of this study include the limited sample size and the scarcity of NPR samples. The lack of other pathological response subgroups restricts the further identification of differential cell clusters associated with treatment response or resistance. By comparing the differences between pre- and posttreatment primary tumor samples and metastatic lymph nodes from patients with a pCR or NPR, we identified potential targets for the resistance to NACI in OSCC. However, how these findings relate to the mechanisms of NACI requires further investigation. Additionally, techniques such as immunohistochemistry or immunofluorescence were not used to validate the results, so further verification is needed.

Conclusion

In conclusion, we characterized the immune landscape of OSCC primary tumors and metastatic lymph nodes within the context of clinical response to NACI. These findings provide important insights for better understanding patient responses to treatment and for identifying potential new therapeutic targets for future OSCC therapies.

Supplementary Information The online version contains supplementary material available at https://doi.org/10.1007/s00262-025-04014-2.

Acknowledgements Not applicable.

Author contributions Jie Zhang contributed to the study conception and design. Material preparation, data collection and analysis were performed by Pu-Gen An, Wen-Jie Wu, Xiao Hu and Zi-Qi Zhang. The first draft of the manuscript was written by Pu-Gen An and Wen-Jie Wu. And all authors commented on previous versions of the manuscript. All authors read and approved the final manuscript.

Funding This work was supported by the Clinical Research Foundation of Peking University School and Hospital of Stomatology (PKUSS-2023CRF1012), the National Key Research and Development Program of China (2022YFC2504203) and the Beijing Xisike Clinical Oncology Research Foundation (Y-MSDPU2022-0547).

Data availability All data of this study are available from the corresponding author upon reasonable request.

Declarations

Conflict of interest The authors declare that they have no conflict of interest.

Ethics approval and consent to participate The four patients originated from a clinical trial, which was approved by the Ethics Committee of Peking University School Hospital of Stomatology (PKUSSIRB-202386047), conducted in accordance with the Declaration of

Helsinki and registered at ClinicalTrials.gov (NCT06009861). Written informed consent was obtained from all participants.

References

1. Bray F, Laversanne M, Sung H, Ferlay J, Siegel RL, Soerjomataram I, Jemal A (2024) Global cancer statistics 2022: GLOBOCAN estimates of incidence and mortality worldwide for 36 cancers in 185 countries. CA Cancer J Clin 74:229–263. https://doi.org/10.3322/caac.21834
2. Pulte D, Brenner H (2010) Changes in survival in head and neck cancers in the late 20th and early 21st century: a period analysis. Oncologist 15:994–1001. https://doi.org/10.1634/theoncologist.2009-0289
3. Zanoni DK, Montero PH, Migliacci JC, Shah JP, Wong RJ, Ganly I, Patel SG (2019) Survival outcomes after treatment of cancer of the oral cavity (1985–2015). Oral Oncol 90:115–121. https://doi.org/10.1016/j.oraloncology.2019.02.001
4. Cooper JS, Zhang Q, Pajak TF et al (2012) Long-term follow-up of the RTOG 9501/intergroup phase III trial: postoperative concurrent radiation therapy and chemotherapy in high-risk squamous cell carcinoma of the head and neck. Int J Radiat Oncol Biol Phys 84:1198–1205. https://doi.org/10.1016/j.ijrobp.2012.05.008
5. Li R, Ye L, Zhu Y et al (2022) Induction chemotherapy of modified docetaxel, cisplatin, 5-fluorouracil for laryngeal preservation in locally advanced hypopharyngeal squamous cell carcinoma. Head Neck 44:2018–2029. https://doi.org/10.1002/hed.27119
6. Ghi MG, Paccagnella A, Ferrari D et al (2017) Induction TPF followed by concomitant treatment versus concomitant treatment alone in locally advanced head and neck cancer. A phase II–III trial. Ann Oncol 28:2206–2212. https://doi.org/10.1093/annonc/mdx299
7. Cohen EE, Karrison TG, Kocherginsky M et al (2014) Phase III randomized trial of induction chemotherapy in patients with N2 or N3 locally advanced head and neck cancer. J Clin Oncol 32:2735–2743. https://doi.org/10.1200/jco.2013.54.6309
8. Wakelee H, Liberman M, Kato T et al (2023) Perioperative Pembrolizumab for early-stage non-small-cell lung cancer. N Engl J Med 389:491–503. https://doi.org/10.1056/NEJMoa2302983
9. Forde PM, Spicer J, Lu S et al (2022) Neoadjuvant nivolumab plus chemotherapy in resectable lung cancer. N Engl J Med 386:1973–1985. https://doi.org/10.1056/NEJMoa2202170
10. Yin J, Yuan J, Li Y et al (2023) Neoadjuvant adebrelimab in locally advanced resectable esophageal squamous cell carcinoma: a phase 1b trial. Nat Med 29:2068–2078. https://doi.org/10.1038/s41591-023-02469-3
11. Jiang YZ, Liu Y, Xiao Y et al (2021) Molecular subtyping and genomic profiling expand precision medicine in refractory metastatic triple-negative breast cancer: the FUTURE trial. Cell Res 31:178–186. https://doi.org/10.1038/s41422-020-0375-9
12. Burtness B, Harrington KJ, Greil R et al (2019) Pembrolizumab alone or with chemotherapy versus cetuximab with chemotherapy for recurrent or metastatic squamous cell carcinoma of the head and neck (KEYNOTE-048): a randomised, open-label, phase 3 study. Lancet 394:1915–1928. https://doi.org/10.1016/S0140-6736(19)32591-7
13. Uppaluri R, Campbell KM, Egloff AM et al (2020) Neoadjuvant and adjuvant pembrolizumab in resectable locally advanced, human papillomavirus-unrelated head and neck cancer: a multicentre, phase II trial. Clin Cancer Res 26:5140–5152. https://doi.org/10.1158/1078-0432.Ccr-20-1695
14. Wise-Draper TM, Gulati S, Palackdharry S et al (2022) Phase II clinical trial of neoadjuvant and adjuvant pembrolizumab in resectable local-regionally advanced head and neck squamous cell carcinoma. Clin Cancer Res 28:1345–1352. https://doi.org/10.1158/1078-0432.CCR-21-3351
15. Zhang Z, Wu B, Peng G et al (2022) Neoadjuvant chemoimmunotherapy for the treatment of locally advanced head and neck squamous cell carcinoma: a single-arm phase 2 clinical trial. Clin Cancer Res 28:3268–3276. https://doi.org/10.1158/1078-0432.CCR-22-0666
16. Wu WJ, Liu Q, An PG, Wang L, Zhang JY, Chen Y, Zhang T, Zhang J (2023) Neoadjuvant tislelizumab combined with chemotherapy in locally advanced oral or oropharyngeal squamous cell carcinoma: a real-world retrospective study. Front Immunol 14:1282629. https://doi.org/10.3389/fimmu.2023.1282629
17. Zinner R, Johnson JM, Tuluc M et al (2020) Neoadjuvant nivolumab (N) plus weekly carboplatin (C) and paclitaxel (P) in resectable locally advanced head and neck cancer. J Clin Oncol 38:6583. https://doi.org/10.1200/JCO.2020.38.15_suppl.6583
18. Hecht M, Gostian AO, Eckstein M et al (2020) Safety and efficacy of single cycle induction treatment with cisplatin/docetaxel/ durvalumab/tremelimumab in locally advanced HNSCC: first results of CheckRad-CD8. J Immunother Cancer. https://doi.org/10.1136/jitc-2020-001378
19. Liu B, Hu X, Feng K et al (2022) Temporal single-cell tracing reveals clonal revival and expansion of precursor exhausted T cells during anti-PD-1 therapy in lung cancer. Nat Cancer 3:108–121. https://doi.org/10.1038/s43018-021-00292-8
20. Li J, Wu C, Hu H et al (2023) Remodeling of the immune and stromal cell compartment by PD-1 blockade in mismatch repair-deficient colorectal cancer. Cancer Cell 41:1152–69.e7. https://doi.org/10.1016/j.ccell.2023.04.011
21. Zhao H, Wu L, Yan G, Chen Y, Zhou M, Wu Y, Li Y (2021) Inflammation and tumor progression: signaling pathways and targeted intervention. Signal Transduct Target Ther 6:263. https://doi.org/10.1038/s41392-021-00658-5
22. Gao Y, Li J, Cheng W et al (2024) Cross-tissue human fibroblast atlas reveals myofibroblast subtypes with distinct roles in immune modulation. Cancer Cell 42:1764–83.e10. https://doi.org/10.1016/j.ccell.2024.08.020
23. Herbst RS, Soria JC, Kowanetz M et al (2014) Predictive correlates of response to the anti-PD-L1 antibody MPDL3280A in cancer patients. Nature 515:563–567. https://doi.org/10.1038/nature14011
24. Hegde PS, Karanikas V, Evers S (2016) The where, the when, and the how of immune monitoring for cancer immunotherapies in the era of checkpoint inhibition. Clin Cancer Res 22:1865–1874. https://doi.org/10.1158/1078-0432.Ccr-15-1507
25. Sakaguchi S, Miyara M, Costantino CM, Hafler DA (2010) FOXP3+ regulatory T cells in the human immune system. Nat Rev Immunol 10:490–500. https://doi.org/10.1038/nri2785
26. Wondergem NE, Nauta IH, Muijlwijk T, Leemans CR, van de Ven R (2020) The immune microenvironment in head and neck

squamous cell carcinoma: on subsets and subsites. Curr Oncol Rep 22:81. https://doi.org/10.1007/s11912-020-00938-3
27. Hanahan D, Weinberg RA (2011) Hallmarks of cancer: the next generation. Cell 144:646–674. https://doi.org/10.1016/j.cell.2011.02.013
28. Öhlund D, Elyada E, Tuveson D (2014) Fibroblast heterogeneity in the cancer wound. J Exp Med 211:1503–1523. https://doi.org/10.1084/jem.20140692
29. Gascard P, Tlsty TD (2016) Carcinoma-associated fibroblasts: orchestrating the composition of malignancy. Genes Dev 30:1002–1019. https://doi.org/10.1101/gad.279737.116
30. Koliaraki V, Henriques A, Prados A, Kollias G (2020) Unfolding innate mechanisms in the cancer microenvironment: the emerging role of the mesenchyme. J Exp Med 1:2. https://doi.org/10.1084/jem.20190457
31. Rønnov-Jessen L, Petersen OW, Bissell MJ (1996) Cellular changes involved in conversion of normal to malignant breast: importance of the stromal reaction. Physiol Rev 76:69–125. https://doi.org/10.1152/physrev.1996.76.1.69
32. Delinassios JG, Hoffman RM (2022) The cancer-inhibitory effects of proliferating tumor-residing fibroblasts. Biochim Biophys Acta Rev Cancer 1877:188673. https://doi.org/10.1016/j.bbcan.2021.188673
33. Onder L, Papadopoulou C, Lütge A et al (2024) Fibroblastic reticular cells generate protective intratumoral T cell environments in lung cancer. Cell. https://doi.org/10.1016/j.cell.2024.10.042
34. Mellman I, Chen DS, Powles T, Turley SJ (2023) The cancer-immunity cycle: indication, genotype, and immunotype. Immunity 56:2188–2205. https://doi.org/10.1016/j.immuni.2023.09.011
35. Duraiswamy J, Turrini R, Minasyan A et al (2021) Myeloid antigen-presenting cell niches sustain antitumor T cells and license PD-1 blockade via CD28 costimulation. Cancer Cell 39:1623–42.e20. https://doi.org/10.1016/j.ccell.2021.10.008